Vol. 34 (2003) *ACTA PHYSICA POLONICA B* No 10

SIMULATING RARE EVENTS IN SPIN GLASSES*

Wolfhard Janke

Institut für Theoretische Physik, Universität Leipzig
Augustusplatz 10/11, 04109 Leipzig, Germany
E-mail: `janke@itp.uni-leipzig.de`

Bernd A. Berg

Department of Physics and
School of Computational Science and Information Technology
Florida State University, Tallahassee, FL 32306, USA
E-mail: `berg@hep.fsu.edu`

and Alain Billoire

Service de Physique Théorique, CEA/Saclay
91191 Gif-sur-Yvette, France
E-mail: `billoir@spht.saclay.cea.fr`

(Received August 18, 2003)

We present results of high-statistics Monte Carlo simulations of the three-dimensional Edwards–Anderson Ising spin-glass model. The study is performed with the multi-overlap algorithm, a non-Boltzmann sampling technique which is specifically tailored for sampling rare-event states. This enabled us to study the free-energy barriers $F_{\rm B}^{q}$ in the probability densities $P_J(q)$ of the Parisi overlap parameter q and the far tail region of the disorder averaged density $P(q) = [P_J(q)]_{\rm av}$. In the latter case we find support for extreme order statistics over many orders of magnitude. A comparative study of the three-dimensional pure Ising model shows that this property is special to spin glasses.

PACS numbers: 75.10.Nr, 75.40.Mg, 75.50.Lk

* Presented at the Workshop on Random Geometry, Kraków, Poland, May 15–17, 2003.

1. Introduction

A widely studied class of spin-glass materials [1–4] consists of dilute solutions of magnetic transition metal impurities in noble metal hosts, for instance [5] Au–2.98% Mn. In these systems, the interaction between impurity moments is caused by the polarization of the surrounding Fermi sea of the host conduction electrons, leading to an effective interaction of the so-called RKKY form [6]

$$J_{\mathrm{eff}}(R) \propto \frac{\cos(2k_{\mathrm{F}}R)}{R^3}\,, \qquad k_{\mathrm{F}}R \gg 1\,, \tag{1}$$

where k_{F} is the Fermi wave number. This constitutes the two basic ingredients necessary for spin-glass behavior, namely

- *randomness* — in course of the dilution process the positions of the impurity moments are randomly distributed, and
- *competing interactions* — due to the oscillations in (1) as a function of the distance R between the spins, some of the interactions are positive and some are negative.

The competition among the different interactions between the moments means that no single configuration of spins is favored by all of the interactions, a phenomenon which is called "frustration". This leads to a rugged free-energy landscape with probable regions (low free energy) separated by rare-event states (high free energy), illustrated in many previous articles by sketches similar to our Fig. 1. Experimentally this may be inferred from the phenomenon of aging observed in measurements of the remanent magneti-

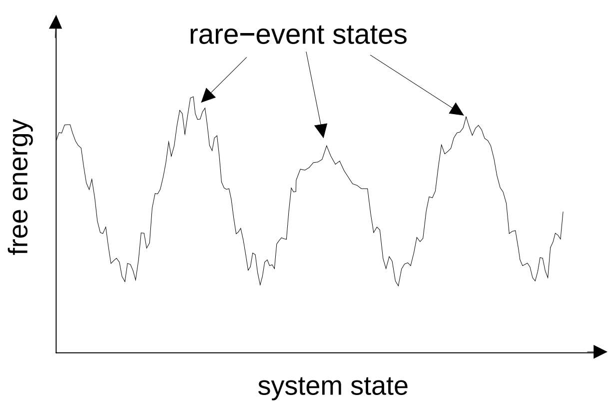

Fig. 1. Typical sketch of the rugged free-energy landscape of spin glasses, with many minima separated by rare-event barriers.

zation in the spin-glass phase. Despite the large amount of experimental, theoretical and simulational work done in the past thirty years to elucidate the nature of the spin-glass phase [1–4], the physical mechanisms underlying its peculiar properties are not yet fully understood.

The purpose of this note is to give an overview of our results in three dimensions. In Sec. 2 we define the model and its observables, in particular the overlap order parameter, and describe the multi-overlap algorithm employed in the Monte Carlo simulations. Section 3 is devoted to our results on the distribution of free energy barriers, on the tails of the averaged probability distribution of the overlap parameter and of a comparative study of the three-dimensional Ising model. Finally, in Sec. 4 we close with a summary and an outlook to future work.

2. Lattice models and simulation method

To cope with the complexity of the problem various levels of simplified models have been proposed. A minimalistic lattice model which reflects the two basic ingredients for spin-glass behavior is the Edwards–Anderson [7] Ising (EAI) model with Hamiltonian

$$H = -\sum_{\langle ik \rangle} J_{ik}\, s_i s_k \,, \tag{2}$$

where the lattice sum runs over all nearest-neighbour pairs of a d-dimensional (hyper-) cubic lattice of size $N = L^d$ with periodic boundary conditions, $s_i = \pm 1$ are Ising spins, and the J_{ik} are quenched coupling constants taking *randomly* positive and negative signs, thereby leading to *competing interactions*. In our study we worked with a bimodal distribution, $J_{ik} = \pm 1$ with equal probabilities.

A mean-field tractable model, the Sherrington–Kirkpatrick [8] model, emerges when each spin is allowed to interact with all others. Alternatively one may consider the mean-field treatment as an approximation which is expected to become accurate in high dimensions [9]. In physical dimensions, however, its status is still unclear and the alternative droplet model [10] has been proposed. The two treatments yield conflicting predictions. Numerical approaches such as Monte Carlo (MC) simulations can, in principle, provide precise results in physical dimensions and hence can help to decide between the two theories. In practice, however, the simulational approach is severely hampered by an extremely slow dynamics of the stochastic process, and the need to consider many disorder realizations.

To overcome the slowing-down problem various ingenious simulation techniques have been devised in the past few years. While some of them only aim at improving the dynamics of the MC process, others are in addition well suited for a quantitative characterization of the free-energy barriers responsible for the slowing-down problem. Among the latter category is the multi-overlap algorithm [11] which has been employed in our MC simulations [12, 13] of the EAI spin-glass model.

Following Parisi [9] one usually takes as order parameter the overlap

$$q = \frac{1}{N} \sum_{i=1}^{N} s_i^{(1)} \, s_i^{(2)} \, , \tag{3}$$

where the spin superscripts label two independent (real) replicas for the same disorder realization $J = \{J_{ik}\}$. For a given J the probability density of q is denoted by $P_J(q)$, and thermodynamic expectation values are computed as

$$\langle \ldots \rangle_J \equiv \sum_{\{s\}} (\ldots) \exp(-\beta H[J]) \Bigg/ \sum_{\{s\}} \exp(-\beta H[J]) \ , \tag{4}$$

where $\beta = 1/T$ is the inverse temperature in natural units. The freezing temperature is known to be at $\beta_{\rm c} = 0.90(3)$ [14].

The results depend on the randomly chosen quenched coupling constants, and one must average over many hundreds or even thousands of disorder realizations:

$$P(q) = [P_J(q)]_{\rm av} = \frac{1}{\#J} \sum_J P_J(q) \, , \qquad [\langle \ldots \rangle_J]_{\rm av} = \frac{1}{\#J} \sum_J \langle \ldots \rangle_J \, , \tag{5}$$

where $\#J$ ($\to \infty$) is the number of realizations. Below the freezing temperature, in the infinite-volume limit $N \to \infty$, a non-vanishing part of $P(q)$ between its two delta-function peaks at $\pm q_{\rm max}$ characterizes the mean-field picture [9] of spin glasses, whereas in the droplet picture [10] of spin glasses (as well as in ferromagnets) $P(q)$ exhibits only the two delta-function peaks.

For a better understanding of the free-energy barriers sketched in Fig. 1, the probability densities for *individual* realizations J play the central role. As it is impossible to get complete control over the full state space, and to give a well-defined meaning to the “system state” (the x-axis in Fig. 1), one has to concentrate on one or a few characteristic properties. In our work we focused on the order parameter q and thus on those free-energy barriers $F_{\rm B}^q$ which are reflected by the minima of $P_J(q)$. Conventional, canonical MC simulations are not suited for this problem since the likelihood to generate the corresponding rare-event configurations in the Gibbs canonical ensemble is very small. This problem is overcome by non-Boltzmann sampling with the multi-overlap weight [11]

$$w_J(q) = \exp\left[\beta \sum_{\langle ik\rangle} J_{ik}\left(s_i^{(1)}s_k^{(1)} + s_i^{(2)}s_k^{(2)}\right) + S_J(q)\right] , \tag{6}$$

where the two replicas are coupled by $S_J(q)$ in such a way that a broad multi-overlap histogram $P_J^{\mathrm{muq}}(q)$ over the entire accessible range $-1 \le q \le 1$ is obtained. When simulating with the multi-overlap weight (6), canonical expectation values of any quantity O can be reconstructed by reweighting, $\langle O\rangle_J^{\mathrm{can}} = \langle O\mathrm{e}^{-S_J}\rangle_J / \langle \mathrm{e}^{-S_J}\rangle_J$.

For each of the quenched disorder realizations the steps of the multi-overlap algorithm may be summarized as follows:

- An iterative construction of the weight function $W_J(q) \equiv \exp(S_J(q))$;
- an equilibration period with fixed weight function;
- a production run with fixed weight function.

Notice that the multi-overlap as defined in Ref. [15] is slightly different, and in this context our present algorithm could be termed "multi-self-overlap".

We measure the dynamics of the multi-overlap algorithm by means of the autocorrelation time τ_J^{muq}, which is defined by counting the average number of sweeps it takes to complete the cycle $q = 0 \to |q| = 1 \to q = 0$. Adopting the usual terminology [16] for a first-order phase transition, we shall call such a cycle a "tunneling" event. The weight iteration was stopped after at least 10 "tunneling" events occurred, and in the production runs we collected at least 20 "tunneling" events. To allow for standard reweighting in the temperature we stored besides $P_J(q)$ also the time series of q, and of the energies and magnetizations of the two replicas. The number of sweeps between measurements was adjusted by an adaptive data compression routine to ensure that each time series consists of $2^{16} = 65\,536$ measurements separated by approximately τ_J^{muq} sweeps.

3. Results

Our simulation temperatures of the three-dimensional (3D) model were $T = 1 \approx 0.88\,T_\mathrm{c}$ and $T = 1.14 \approx T_\mathrm{c}$. In the spin-glass phase at $T = 1$ we simulated 8192 disorder realizations for $L = 4$, 6, and 8, and 640 realizations for $L = 12$. At the freezing temperature the corresponding numbers are again 8192 for $L = 4$, 6, and 8, 1024 for $L = 12$, and 256 for $L = 16$.

Due to the large number of realizations simulated, the final results are relatively costly. By fitting the averaged autocorrelation times to the power-law ansatz $\ln([\tau_J^{\rm muq}]_{\rm av}) = a + z\,\ln(N)$, we obtained [12] $z = 2.32(7)$. The quality of the fit is poor and an exponential behavior ($\ln([\tau_J^{\rm muq}]_{\rm av}) \propto N^{\alpha}$) cannot be excluded. This shows that the slowing down is quite off from the theoretical optimum $z = 1$, one would expect if the multi-overlap autocorrelation time $\tau_J^{\rm muq}$ was dominated by a random-walk behavior between $q = -1$ and $+1$. In multicanonical simulations with broad *energy* histograms an even larger exponent of $z = 2.8(1)$ has been observed [17]. The large values of z suggest that barriers in the canonical overlap or energy are not the exclusive cause for the slowing down of spin-glass dynamics below the freezing point. The projection of the multi-dimensional state space onto the q- or E-direction averages out most of the free-energy landscape of the model. Barriers in other directions may thus be hidden, as was recently elucidated in the context of multi-magnetical simulations of the two-dimensional Ising model in the low-temperature phase [18].

3.1. Free-energy barriers $F_{\rm B}^q$

The behavior of the free-energy barriers $F_{\rm B}^q$ depends on the shape of the individual probability densities $P_J(q)$. To allow for a visual inspection of the encountered shapes, all 640 probability densities $P_J(q)$ at $T = 1 \approx 0.88\,T_{\rm c}$ for the 12^3 lattice have been made available through a Java animation as a "picture show" on the Web [19]. To define effective free-energy barriers $F_{\rm B}^q$ we first constructed [12] an auxiliary 1D Metropolis–Markov chain which has the canonical $P_J(q)$ probability density as its equilibrium distribution. The tridiagonal transition matrix of this Markov process allows for diagonalization by standard methods. The largest eigenvalue λ_0 equals unity and is non-degenerate. The second largest eigenvalue λ_1 determines the autocorrelation time (in units of sweeps) of the chain,

$$\tau_{\rm B}^q = -\frac{1}{N\ln\lambda_1} \approx \frac{1}{N(1-\lambda_1)}\,, \tag{7}$$

which we use to define for each disorder realisation an associated *effective* free-energy barrier in the overlap parameter q as

$$F_{\rm B}^q \equiv \ln(\tau_{\rm B}^q)\,. \tag{8}$$

In our finite-size scaling (FSS) analyses we concentrated on the density $\mathcal{P}$ of the overlap barriers or, more precisely, its (cumulative) distribution function $F(x) = \int_0^x dx'\mathcal{P}(x')$. The reason is that, in contrast to the energy, the thus defined free-energy barriers are non-self-averaging. In this case one

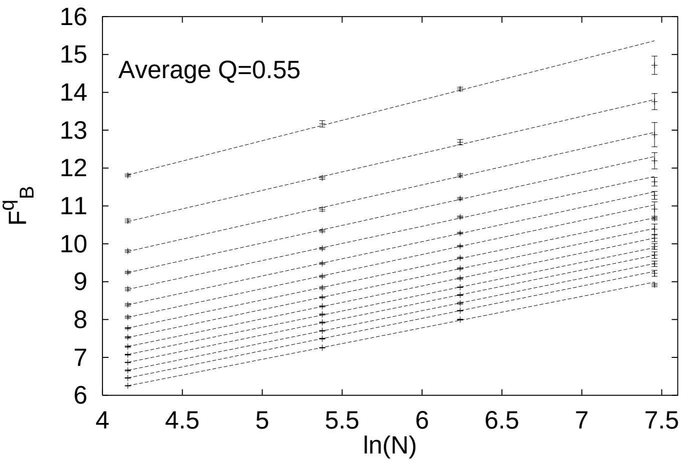

Fig. 2. FSS fits of the overlap barriers F_{B}^{q} in the spin-glass phase at $T = 1$ for fixed values of the distribution function, $F = i/16$, $i = 1, \ldots, 15$ (from bottom to top). Shown are the results for the ansatz (10).

has to investigate many samples and should report the FSS behavior for fixed values of F. Assuming an ansatz suggested by mean-field theory [20, 21],

$$F_{\mathrm{B}}^{q} = a_1 + a_2\, N^{1/3}\,, \tag{9}$$

corresponding to $\tau_{\mathrm{B}}^{q} \propto \exp(a_2\, N^{1/3})$, we hence performed [12] FSS fits for $F = i/16$, $i = 1, \ldots, 15$. The quality of the fits, however, turned out to be poor with an unacceptably small average goodness-of-fit parameter $Q = 0.0002$. We therefore also tried fits to the ansatz

$$F_{\mathrm{B}}^{q} = c + \alpha\, \ln(N)\,, \tag{10}$$

corresponding to $\tau_{\mathrm{B}}^{q} \propto N^{\alpha}$. As can be seen in Fig. 2, they yield much better results with the exponent $\alpha = \alpha(F)$ varying smoothly from 0.8 to 1.1 for $F = 1/16$ to 15/16. A similar analysis [12] for the autocorrelation times τ_J^{muq} gives larger exponents $\alpha^{\mathrm{muq}}(F) \approx \alpha_{\mathrm{B}}^{q}(F) + 1$, indicating again the presence of other relevant barriers that cannot be detected in the overlap parameter q.

3.2. Averaged probability densities $P(q)$

At least close to T_{c} one expects that, up to finite-size corrections, the probability densities scale with system size L. This may be visually confirmed by plotting $P'(q) \equiv \sigma P(q)$ *versus* $q' = q/\sigma$, where $\sigma \propto L^{-\beta/\nu}$ is the standard deviation. From least-square fits we obtained [13] $\beta/\nu = 0.312(4)$

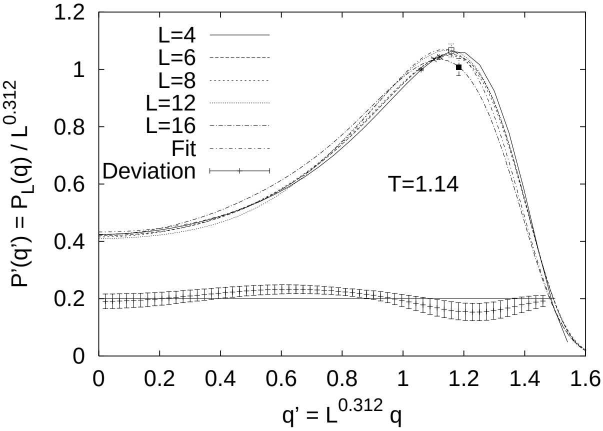

Fig. 3. Rescaled overlap probability densities for the EAI spin-glass model on L^3 lattices at the transition temperature. In the lower part the deviation $P'(q') - P'_{\rm fit}(q') \pm \triangle P'(q')$ of some $L = 16$ data from the modified Gumbel fit is shown (offset by 0.2 to fit inside the figure).

($Q = 0.32$) for $T = 1.14$ and $\beta/\nu = 0.230(4)$ ($Q = 0.99$) for $T = 1$, respectively. The resulting scaling plot for $T = 1.14$ in Fig. 3 demonstrates that the five probability densities indeed collapse onto a single master curve. Remarkably, this still holds true at $T = 1$ below the critical point [13].

The multi-overlap algorithm becomes particularly powerful when studying the tails of the probability densities which are highly suppressed compared to the peak values. This is illustrated in Fig. 4 which shows $P(q)$ at $T = 1.14$ on a logarithmic scale over more than 150 orders of magnitude. Based on the replica mean-field approach, the tails have been predicted [22] to follow for $q > q^{\infty}_{\rm max}$ a scaling behavior of the form $P(q) = P_{\rm max}\, f(N\,(q - q^{\infty}_{\rm max})^x)$ which, for large arguments of f, should approach

$$P(q) \sim \exp\left[-c_1\, N\,(q - q^{\infty}_{\rm max})^x\right] , \tag{11}$$

with a mean-field exponent of $x = 3$. By allowing for an overall normalization factor $c_0^{(N)}$, taking the logarithm twice and performing fits of the form [23]

$$Y \equiv \ln\left[-\ln\left(P/c_0^{(N)}\right)\right] - \ln N = \ln c_1 + x\, \ln(q - q^{\infty}_{\rm max})\,, \tag{12}$$

we obtained consistent fits only over a rather restricted range of q. Using them anyway, and leaving the exponent x as a free parameter, we arrived at the estimate $x = 12\,(2)$, which is much larger than the mean-field value of $x = 3$.

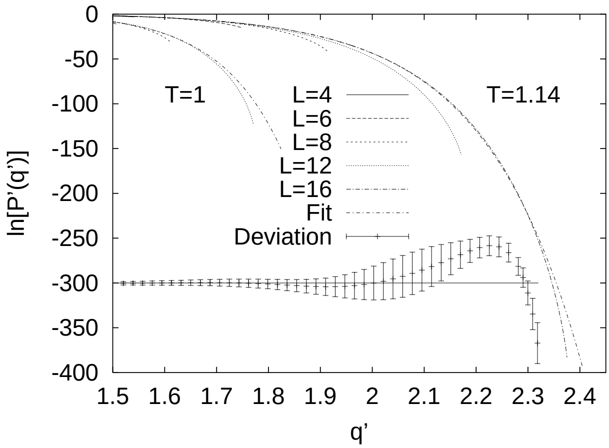

Fig. 4. Tails of the rescaled overlap probability densities for the EAI spin-glass model on L^3 lattices at the critical temperature on a logarithmic scale. In the lower part of the plot the deviation $P'(q') - P'_{\rm fit}(q') \pm \triangle P'(q')$ of some $L = 16$ data from the modified Gumbel fit is shown (with an unimportant offset added in order to be inside the figure).

By looking for reasonable alternatives we realized that for the 2D XY model the *statistics of extremes* (or, equivalently, *extreme order statistics*) has led to a good ansatz with universal properties [24, 25]. This ansatz is based on a standard result [26, 27], due to Fisher and Tippett, Kawata, and Smirnov, for the universal distribution of the first, second, third, ... smallest of a set of N independent, identically distributed random numbers. For an appropriate, exponential decay of the random number distribution their probability densities are given by the Gumbel form

$$f_a(x) \;=\; C_a \exp\left[\, a \;(x - \mathrm{e}^x\,)\right] \tag{13}$$

in the limit of large N. The exponent a takes the values $a = 1, 2, 3, \ldots$, corresponding, respectively, to the first, second, third, ... smallest random number of the set, x is a scaling variable which shifts the maximum value of the probability density to zero, and C_a is a normalization constant. For certain spin-glass systems the possible relevance of this universal distribution has been pointed out by Bouchaud and Mézard [28]. For the 2D XY model in the spin-wave approximation [24,25] a modified Gumbel ansatz (13) emerges with a value of $a = \pi/2$.

In our case we set $x = b(q' - q'_{\rm max})$ and modified the first x on the r.h.s. of (13) to $c \tanh(x/c)$, where $c > 0$ is a constant, in order to reproduce the flattening of the densities towards $q' = 0$. The important large-x behavior of Eq. (13) is not at all affected by this manipulation. By fitting this ansatz to our data we obtained final estimates [13] of $a = 0.448\,(40)$ for $T = 1.14$ and $a = 0.446\,(37)$ for $T = 1$, respectively. The fits are depicted in Fig. 4, and for $T = 1.14$ our fit is also included in Fig. 3. We see a good consistency between the data and the fit over a remarkably wide range of q'. Most impressive is the excellent agreement in the tails of the densities. Taking the $T = 1.14$, $L = 16$ result at face value, we find a very good description over the remarkable range of $200/\ln(10) \approx 87$ orders of magnitude.

3.3. Comparison with $P(q)$ of the 3D Ising model

By simply setting all coupling constants J_{ik} to one, we have used exactly the same simulation set-up for studying the 3D Ising model at its critical point [29] $\beta_{\rm c} = 0.221\,654$. Here we performed 32 independent runs (with different pseudo random number sequences) for lattices up to size $L = 30$ and 16 independent runs for $L = 36$ [30]. After calculating the multi-overlap parameters [11] the following numbers of sweeps were performed per repetition (*i.e.* independent run): $2^{19}, 2^{21}, 2^{22}, 2^{23}, 2^{23}, 2^{24}, 2^{25}$, and 2^{24} for $L = 4, 6, 8, 12, 16, 24, 30$, and 36, respectively.

In contrast to the well known double-peak structure of the magnetization probability density of the 3D Ising model at $T_{\rm c}$, we find for the $P_L(q)$ densities a single peak at $q_{\rm max} = 0$ [30]. On a logarithmic scale the tail of the normalized $L = 36$ density continues to exhibit accurate results down to -1200, thus the data from this system cover $1200/\ln(10) = 521$ orders of magnitude. The collapse of the $P_L(q)$ functions on one universal curve $P'(q')$ is depicted in Fig. 5. The figure shows some scaling violations, which become rather small from $L \geq 24$ onwards. The standard deviation σ_L behaves with L according to $\sigma_L \propto L^{-2\beta/\nu}\,(1 + c_2 L^{-\omega} + \ldots)$, and from fits to our data we obtained $2\beta/\nu = d - 2 + \eta = 1.030(5)$, in good agreement with FSS estimates for the magnetization [31] which cluster around $\eta = 0.036$.

We compared fits of the data with the Gumbel form (13) and the standard large-deviation behavior,

$$P_L(q) \propto \exp[-N f(q)]\,. \tag{14}$$

The proportionality of the entropy with the volume implies that, for large N, $f(q)$ does not depend on N. As is demonstrated in Fig. 6, our data for $f(q)$ clearly support the prediction (14). Also shown is the scaling form $f(q) \propto q^{d\nu/2\beta}$ with $2\beta/\nu = 1.030$. We see excellent convergence towards an L-independent function, but the scaling behavior only holds in the vicinity of $q = 0$.

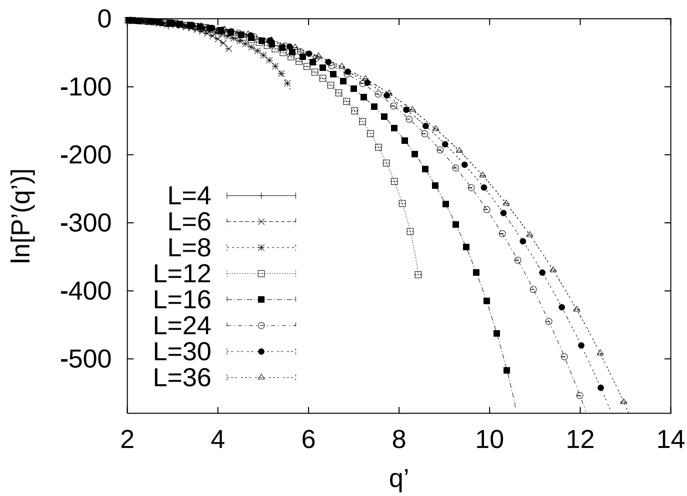

Fig. 5. Rescaled overlap probability densities $P'(q') = \sigma_L \, P_L(q)$ on a logarithmic scale *versus* $q' = q/\sigma_L$ for the 3D Ising model at the critical point.

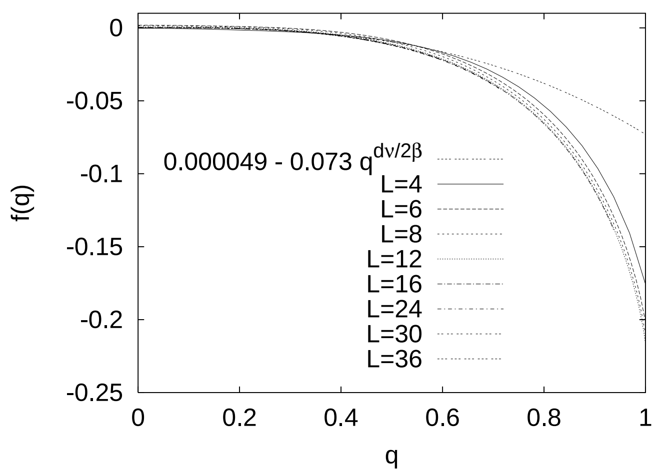

Fig. 6. The function $f(q)$ extracted from the large-deviation behavior (14) for the 3D Ising model and various lattice sizes. Also shown is a FSS fit valid for small q.

4. Summary and conclusions

Employing non-Boltzmann sampling with the multi-overlap MC algorithm we have investigated for the 3D EAI spin-glass model the probability densities $P_J(q)$ of the Parisi order parameter q. The free-energy barriers $F_{\rm B}^q$ as defined in Eq. (8) turn out to be non-self-averaging. The logarithmic scaling ansatz (10) for the barriers at fixed values of their cumulative distribution function F is found to be favored over the mean-field ansatz (9). Further, relevant barriers are still reflected in the autocorrelations of the multi-overlap algorithm.

The averaged densities $P(q)$ exhibit a good FSS collapse onto a L-independent master curve at and slightly below the critical temperature. For the scaling of their tails towards $q = \pm 1$ we find no agreement with the decay law predicted by mean-field theory. On the other hand, a good fit over more than 80 orders of magnitude is obtained by using a modified Gumbel ansatz, rooted in extreme order statistics [26, 27]. The detailed relationship between the EAI spin-glass model and extreme order statistics remains to be investigated.

For the 3D Ising model at T_c, on the other hand, we do not find evidence for extreme order statistics, in contrast to the suggestions of Refs. [24, 25]. Rather, our results are in good agreement with the standard scaling picture derived from large-deviation theory. We have performed equilibrium simulations of the model. Its critical properties have recently also been studied using non-equilibrium methods [32].

This work was in part supported by the US Department of Energy under contract DE-FG02-97ER41022, the EU-Network HPRN-CT-1999-000161 "EUROGRID – Discrete Random Geometries: From Solid State Physics to Quantum Gravity", and the German-Israel Foundation (GIF) under contract No. I-653-181.14/1999. The numerical simulations were performed on the Compaq SC256 computer of CEA in Grenoble under grant p526 and on the T3E computer of NIC in Jülich under grant hmz091.

REFERENCES

[1] K. Binder, A.P. Young, *Rev. Mod. Phys.* **56**, 801 (1986).

[2] M. Mézard, G. Parisi, M.A. Virasoro, *Spin Glass Theory and Beyond*, World Scientific, Singapore 1987.

[3] K.H. Fischer, J.A. Hertz, *Spin Glasses*, Cambridge University Press, Cambridge 1991.

[4] A.P. Young (ed.), *Spin Glasses and Random Fields*, World Scientific, Singapore 1997.

[5] C.A.M. Mulder, A.J. van Duyneveldt, J.A. Mydosh, *Phys. Rev.* **B25**, 515 (1982).

[6] M.A. Ruderman, C. Kittel, *Phys. Rev.* **96**, 99 (1954); T. Kasuya, *Prog. Theor. Phys.* **16**, 45 (1956); K. Yosida, *Phys. Rev.* **106**, 893 (1957).

[7] S.F. Edwards, P.W. Anderson, *J. Phys. F* **5**, 965 (1975).

[8] D. Sherrington, S. Kirkpatrick, *Phys. Rev. Lett.* **35**, 1792 (1975).

[9] G. Parisi, *Phys. Rev. Lett.* **43**, 1754 (1979).

[10] D.S. Fisher, D.A. Huse, *Phys. Rev.* **B38**, 386 (1988).

[11] B.A. Berg, W. Janke, *Phys. Rev. Lett.* **80**, 4771 (1998).

[12] B.A. Berg, A. Billoire, W. Janke, *Phys. Rev.* **B61**, 12143 (2000).

[13] B.A. Berg, A. Billoire, W. Janke, *Phys. Rev.* **E65**, 045102R (2002).

[14] N. Kawashima, A.P. Young, *Phys. Rev.* **B53**, R484 (1996).

[15] B.A. Berg, H. Noguchi, Y. Okamoto, `cond-mat/0305055`, to appear in *Phys. Rev.* **E**.

[16] B.A. Berg, T. Neuhaus, *Phys. Rev. Lett.* **68**, 9 (1992).

[17] B.A. Berg, U.E. Hansmann, T. Celik, *Phys. Rev.* **B50**, 16444 (1994).

[18] T. Neuhaus, J.S. Hager, `cond-mat/0201324`, to appear in *J. Stat. Phys.*

[19] `http://www.csit.fsu.edu/~ berg/research/complex_systems/complex_systems.html`

[20] N.D. Mackenzie, A.P. Young, *Phys. Rev. Lett.* **49**, 301 (1982); *J. Phys. C* **16**, 5321 (1983); K. Nemoto, *J. Phys. A* **21**, L287 (1988); G.J. Rodgers, M.A. Moore, *J. Phys. A* **22**, 1085 (1989); D. Vertechi, M.A. Virasoro, *J. Phys. (France)* **50**, 2325 (1989).

[21] R.N. Bhatt, S.G.W. Colborne, M.A. Moore, A.P. Young, unpublished, as quoted by Rodgers and Moore (Ref. [20]); see also S.G.W. Colborne, *J. Phys. A* **23**, 4013 (1990); H. Kinzelbach, H. Horner, *Z. Phys.* **B84**, 95 (1991); A. Billoire, E. Marinari, *J. Phys. A* **34**, L727 (2001).

[22] S. Franz, G. Parisi, M.A. Virasoro, *J. Phys. I (France)* **2**, 1869 (1992); G. Parisi, F. Ritort, F. Slanina, *J. Phys. A* **26**, 3775 (1993); J.C. Ciria, G. Parisi, F. Ritort, *J. Phys. A* **26**, 6731 (1993).

[23] W. Janke, B.A. Berg, A. Billoire, in: *Non-Perturbative Methods and Lattice QCD*, Proceedings of the International Workshop, Zhongshan University, Guangzhou (Canton), China, May 15–20, 2000, eds. X.-Q. Luo, E.B. Gregory, World Scientific, Singapore 2001, p. 242.

[24] S.T. Bramwell, K. Christensen, J.-Y. Fortin, P.C.W. Holdsworth, H.J. Jensen, S. Lise, J.M. López, M. Nicodemi, J.-F. Pinton, M. Sellitto, *Phys. Rev. Lett.* **84**, 3744 (2000).

[25] S.T. Bramwell, J.-Y. Fortin, P.C.W. Holdsworth, S. Peysson, J.-F. Pinton, B. Portelli, M. Sellitto, *Phys. Rev.* **E63**, 041106 (2001).

[26] E.J. Gumbel, *Statistics of Extremes*, Columbia University Press, New York 1958.

[27] J. Galambos, *The Asymptotic Theory of Extreme Order Statistics*, 2nd Edition Krieger Publishing, Malabar, Florida 1987.

[28] J.-P. Bouchaud, M. Mézard, *J. Phys. A* **30**, 7997 (1997).

[29] G.S. Pawley, R.H. Swendsen, D.J. Wallace, K.G. Wilson, *Phys. Rev.* **B29**, 4030 (1984).

[30] B.A. Berg, A. Billoire, W. Janke, *Phys. Rev.* **E66**, 046122 (2002).

[31] A. Pelissetto, E. Vicari, *Phys. Rep.* **368**, 549 (2002).

[32] Y. Ozeki, N. Ito, *Phys. Rev.* **B64**, 024416 (2001).